

Article

Study of Gases and Thermal Behavior of Oxidized Coal during Spontaneous Combustion Process

Yan Tang ¹, Wei-Chun Chen ², Hai-Lin Zhou ³, Jing-Yu Zhao ⁴, Chi-Min Shu ⁵  and An-Chi Huang ^{1,*} ¹ School of Safety Science and Engineering, Changzhou University, Changzhou 213164, China² College of Future, National Yunlin University of Science and Technology, Douliu City 64002, Yunlin, Taiwan, R.O.C.³ School of Materials Science and Engineering, Changzhou University, Changzhou 213164, China⁴ School of Safety Science and Engineering, Xi'an University of Science & Technology, Xi'an 710054, China⁵ Department of Safety, Health, and Environmental Engineering, National Yunlin University of Science and Technology, Douliu City 64002, Yunlin, Taiwan, R.O.C.

* Correspondence: huangac@cczu.edu.cn

Abstract: Coal spontaneous combustion is one of the most severe and constant hazards in the coal industry. Understanding the mechanisms is the basis for effective hazard control in the coal-producing process. This paper investigated two types of oxidized coal samples from the re-mining faces of an underground coal mine. Proximate analysis, elemental analysis, surface analysis, temperature-programmed experiments, and differential scanning calorimetry analysis were conducted to study the spontaneous combustion characteristics. Various reaction mechanism functions were adopted to calculate the kinetic parameters, and multiple linear regression was performed to simulate the reaction behavior. The results show that the thermal decomposition of the oxidized coal followed a two-stage reaction model. The first stage reaction occupied smaller apparent activation energy and promoted the second stage reaction, dominating the heat production. Therefore, significant prevention measures for coal spontaneous combustion should be conducted and emphasized appropriately in the first stage to break the continuous reaction. The findings of this study can serve as a reference for predicting and preventing spontaneous combustion of oxidated coal.

Keywords: proximate analysis; elemental analysis; differential scanning calorimetry; mechanism functions; multiple linear regression



Citation: Tang, Y.; Chen, W.-C.; Zhou, H.-L.; Zhao, J.-Y.; Shu, C.-M.; Huang, A.-C. Study of Gases and Thermal Behavior of Oxidized Coal during Spontaneous Combustion Process. *Processes* **2022**, *10*, 1849. <https://doi.org/10.3390/pr10091849>

Academic Editor: Maria Mitu

Received: 20 August 2022

Accepted: 12 September 2022

Published: 14 September 2022

Publisher's Note: MDPI stays neutral with regard to jurisdictional claims in published maps and institutional affiliations.



Copyright: © 2022 by the authors. Licensee MDPI, Basel, Switzerland. This article is an open access article distributed under the terms and conditions of the Creative Commons Attribution (CC BY) license (<https://creativecommons.org/licenses/by/4.0/>).

1. Introduction

Coal spontaneous combustion has long been a worldwide problem in many coal-producing countries, such as China, the United States, Germany, India, Australia, and other areas [1–5]. It frequently occurs in the processes of coal mining, storage, and transportation, bringing detrimental effects to humans and causing severe financial and environmental losses for society [6–11]. Global attention has been paid, and investigations on the mechanisms of coal spontaneous combustion have been conducted extensively by experimental and simulation methods [1,2,12–14]. From a small-scale perspective, the variation of functional groups, molecule structure, thermal stability, and kinetic parameters of coal during the spontaneous combustion process have been studied [15–20]. The effects of various influencing factors, such as moisture, oxygen concentration, metamorphic grade, particle size, and pore volume, have been systematically analyzed [21–24]. From a large-scale perspective, the similarity simulation experimental platforms and multi-field coupling models were successfully developed to investigate the occurrence and development of coal spontaneous combustion [25–30]. The characteristics of temperature evolution, hot spot propagation, heat release, gas consumption, and generation were obtained during the research [28–32].

The previous investigations significantly help the in-depth understanding of coal spontaneous combustion. However, as coal oxidation and combustion are incredibly complicated, a uniform agreement on the reaction process between coal and oxygen has yet been reached [1], and further research is still needed on the spontaneous combustion mechanism of coal. Particularly, many scholars have found that re-mining coal mine with oxidized coal is much easier to return to an accident again in actual situations [33]. Therefore, in this paper, the spontaneous combustion characteristics of two kinds of oxidized coal were investigated using experimental approaches, including proximate and elemental analysis, characteristic surface analysis, thermal analysis, and temperature-programmed experimental analysis. Additionally, differential scanning calorimetry (DSC) and thermokinetic methods were used in this study to estimate the thermokinetic parameters of the oxidized coal, and the heat release behavior of cells during heating was examined. The Achar differential and Coats–Redfern integral methods were used to analyze the thermal response behavior of the oxidized coal throughout the heating process. This study can provide a theoretical basis for preventing and controlling the coal spontaneous combustion.

2. Experimental

2.1. Coal Samples

The oxidized gas-fat coal and 1/3 coking coal samples were used in the experiments. Before being transferred to the lab for sealing and preservation, the samples were sealed and packaged in multi-layer plastic and nylon bags. To ensure test reproducibility, each experiment was run three times. One set of data was then chosen for analysis.

Pieces of fresh coal were pulverized into mixed size samples: 0–0.9, 0.9–3.0, 3.0–5.0, 5.0–7.0, and 7.0–10.0 mm. Moreover, the particle size of 0.075–0.105 mm with a mass of 50 g fresh coal samples was prepared. The mixed coal sample and 0.075–0.105 mm coal samples were put into the temperature-programmed instrument. Then the oxidation heating process started from room temperature (20 °C) to the maximum temperature (170 °C), which the instrument could reach.

2.2. Proximate and Elemental Experiments

The particle size of 0.075–0.105 mm coal samples were tested by proximate and elemental experimental [34,35]. Proximate experimental (5E-MAG6700, Kaiyuan, China) was the primary method to acquire moisture, ash, and volatile contents [36]. The C, H, O, N, and S contents were received by elemental experiments (Vario EL III, Elementar, Hanau, Germany) [37]. The two trials can be used to determine the ranks of coal. Experiments were carried out at standard atmospheric pressure.

2.3. Physical Adsorption Experiments

Physical adsorption could occur on any solid surface because of the van der Waals force between two molecules. Pore volume and specific surface area serve as the physical adsorption indexes. The test tube was placed in a 623 °C liquid nitrogen atmosphere while the Autosorb-IQ-C apparatus from Quantachrome, USA, was used to measure the condensation of gas molecules in solid surfaces and gaps.

2.4. Temperature-Programmed Experimental System

The temperature-programmed system was used to achieve the coal oxidization. The volume of the temperature-programmed box was 50 × 40 × 30 cm, and the test tube was 10 cm in diameter and 25 cm in length. 2 cm of freedom space was left at the top and the end to keep the tested tube ventilated. The component and concentration of gas released during the heating process were measured. The test air flow rate was 120 mL/min, and the heating rate was 0.3 °C/min.

2.5. Differential Scanning Calorimetry (DSC)

DSC was taken to calculate the enthalpy during the procedure of temperature rise [38]. The DSC curves indicated heat effect in different temperatures, and the integral area expressed the heat release [39]. DSC of Mettler Toledo (Zurich, Switzerland) was used for a non-isothermal experiment with a heating rate of 5 °C/min, and the heating range was set from 30 to 800 °C.

3. Results and Discussion

3.1. Coal Quality Analysis

Coal is made up of organic matter and a small amount of minerals. A coal quality study revealed the fundamental elements and chemical makeup of coal [40]. The element proportion of the samples is depicted in Figure 1. Compared to oxidized 1/3 coking coal, the oxidized gas-fat coal has less C, V_{ad} , and FC_{ad} . It implies that 1/3 of coking coal has a high rank. On the contrary, the difficulty of absorbing oxygen resulted in high-rank coal holding less O content than the lower one. Because of the pre-oxidation, the moisture content of coal decreased.

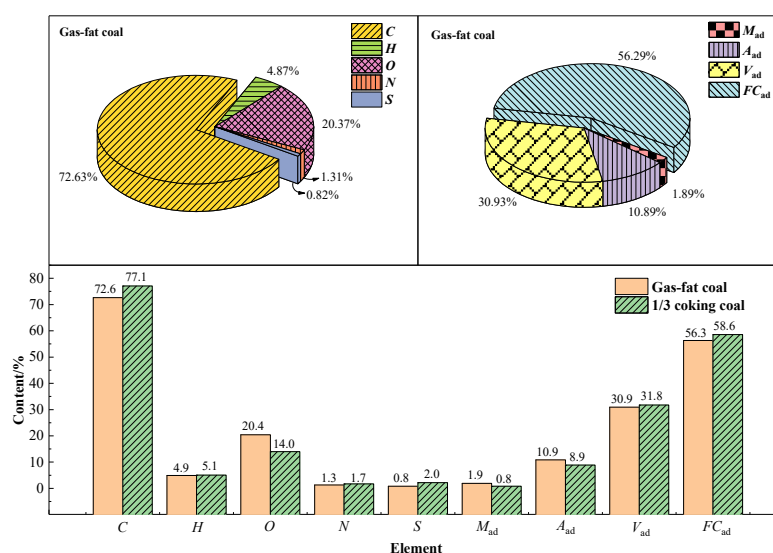


Figure 1. Proximate and elemental experimental analysis.

3.2. Surface Characteristic Analysis

According to the size of pore volume, coal pores could be divided into three types: micropores, medium pores, and large pores [41]. Among them, the diameter of micropores, medium pores, and large pores were less than 2 nm, between 2 to 50 nm, and larger than 50 nm, respectively. The micropore, medium pore, and large pore in the gas-fat coal were 45%, 35%, and 20%, respectively. Compared with gas-fat coal, there were more large pores and fewer micro and medium pores in 1/3 of coking coal. The micropore, medium pore, and large pore in the 1/3 coking coal are 42%, 31%, and 27%, respectively. Moreover, the specific surface area of gas-fat coal is 1.37 m²/g, while the value of 1/3 coking coal is only 0.84 m²/g. The findings indicate that the 1/3 coking coal had relatively stable coal structure characteristics.

3.3. Spontaneous Combustion Characteristic Parameters

Spontaneous combustion parameters include index gases, characteristic temperatures, and oxygen consumption rate. The concentration of index gases indicated the oxidation degree of spontaneous combustion. Characteristic temperatures are the main features of alert hazard points during coal spontaneous combustion. Finally, the oxygen consumption rate expressed the oxidability of coal [42].

3.3.1. Concentration of Index Gases

Gases produced by oxidation from different rank coals were not all the same [43]. Coal and oxygen interacted throughout the low-temperature oxidation process by physical adsorption, chemical adsorption, and chemical reaction. As a result, each stage of gas creation has a unique set of components. Nevertheless, CO, CO₂, CH₄, C₂H₄, and C₂H₆ are the common gases that could be detected in the oxidation process. Wherein CO and C₂H₄ are the index gases that emerge in the coal oxidation, instead of other gases' uncertainty of either self-contains or oxidized produces. The concentration of CO and C₂H₄ gases are shown in Table 1 and Figure 2, respectively.

Table 1. CO concentration versus temperature.

| Temperature (°C) | CO (ppm) | |
|------------------|--------------|-----------------|
| | Gas-Fat Coal | 1/3 Coking Coal |
| 30 | 24.53 | 9.55 |
| 40 | 24.25 | 21.53 |
| 50 | 48.87 | 48.96 |
| 60 | 75.97 | 74.83 |
| 70 | 131.00 | 158.90 |
| 80 | 200.90 | 310.50 |
| 90 | 348.80 | 491.70 |
| 100 | 574.30 | 904.00 |
| 110 | 898.10 | 1248.00 |
| 120 | 1403.00 | 1790.00 |
| 130 | 2114.00 | 2995.00 |
| 140 | 3403.00 | 5059.00 |
| 150 | 5045.00 | 7039.00 |
| 160 | 7442.00 | 10,340.00 |
| 170 | 9992.00 | 13,080.00 |

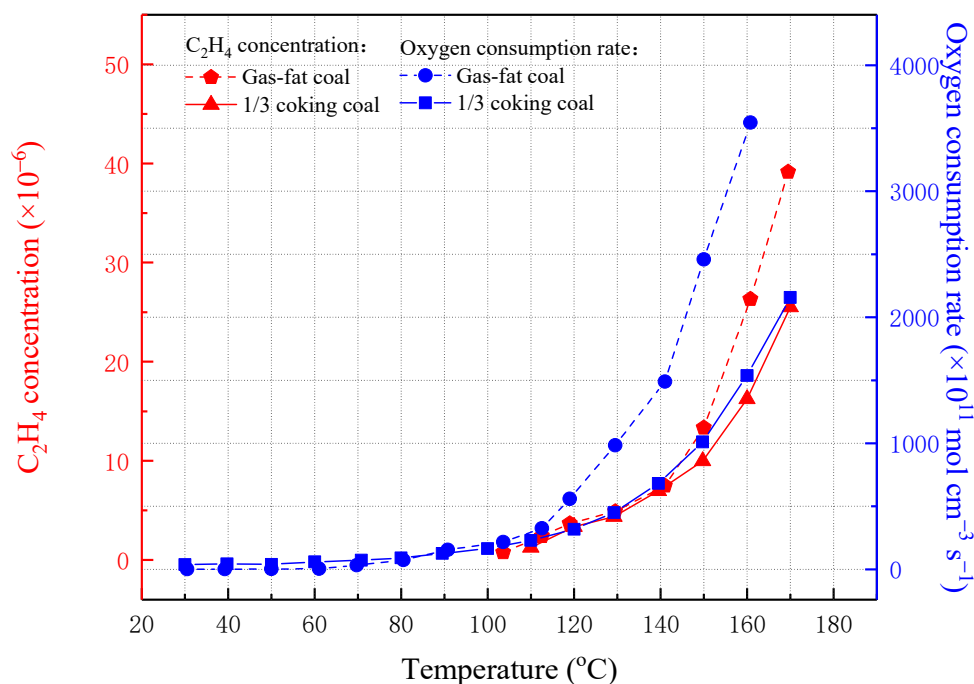


Figure 2. The curve of C₂H₄ concentration and oxygen consumption rate versus temperature.

CO concentration increased as the temperature rose. As to gas-fat coal, CO concentration was amplified very tardily and lower than 1000 ppm at an early oxidation stage (under 70 °C). However, when the heating temperature increased from 70 to 100 °C, CO

concentration began to grow faster and rose rapidly after 100 °C. A similar variation can be found in the data of gas-fat coal; the CO concentration of 1/3 coking coal increased slowly prior to 80 °C. Then, the concentration started to grow quickly from 80 to 110 °C and straightly climbed after 110 °C.

C₂H₄ was the product of spontaneous combustion at the crack temperature [34]. Gas-fat coal and 1/3 coking coal generated C₂H₄ at 110 and 100 °C, respectively. It corresponded to the concentration of CO increasing rapidly. In addition, the gas concentrations of 1/3 coking coal were lower than gas-fat coal as it had a higher rank.

Coal spontaneous combustion is also the main ignition source of gas explosion disaster in goaf [44], and the aforementioned CO and C₂H₄ also have significant effects on the explosion limit of the explosive gas mixture. Previous work has shown that both the lower explosive limit (LEL) and upper explosive limit (UEL) of the gas mixture increased as the CO content rises. However, with the increase in C₂H₄ content, the LEL decreases while the UEL increases [45]. Therefore, the detection of CO and C₂H₄ could provide a theoretical basis for analyzing the coal–oxygen reaction process and the design of prevention measures for gas explosions.

3.3.2. Characteristic Temperatures

Active functional groups and structures in coal molecules transformed drastically at a particular temperature. Gases concentration showed the transformation as macro-performance at a critical temperature. The critical temperature is crucial, indicating that spontaneous combustion would expand to a relatively acute stage and enter the accelerated reaction. The lower the critical temperature is, the higher pyrophoricity is. Crack temperature is a symbolic temperature to caution that the oxidation would speed up directly. At crack temperature, some stable, functional groups began reacting with oxygen, generating a large amount of gases, especially alkene.

Growth rate analysis of index gases was used to calculate the characteristic temperatures of gas-fat coal and 1/3 coking coal, which were shown as follows:

$$Z = \frac{C_{i+1} - C_i}{C_i(t_{i+1} - t_i)} \quad (1)$$

wherein c is the gas concentration (ppm), t is the temperature (s), i is the discretional point from the experimental date, and Z is the growth rate of gas concentration. So, for Gas-fat coal, the critical and crack temperatures are 70 and 100 °C, respectively. The characteristic temperatures of gas-fat coal are lower than 1/3 of coking coals. The 1/3 coking coal has critical and crack temperatures of 80 and 110 °C, respectively.

3.3.3. Oxygen Consumption

The oxygen consumption rate can be obtained as below [25]:

$$V_0(T) = \frac{QC_0}{S(z_2 - z_1)} \ln \frac{C_1}{C_2} \quad (2)$$

where $V_0(T)$ is the oxygen consumption rate of coal in fresh air (mol cm⁻³ s), Q is experimental air volume (cm³ s⁻¹), C_0 represents the standard oxygen concentration (ppm), S is the sectional furnace area (cm²), z is the distance of a certain point to the entrance (cm), and oxygen concentration of the specific point is denoted as C (ppm). The curve of oxygen consumption rate and temperature changes are illustrated in Figure 2.

The typical behavior of oxygen consumption rate with temperature was consistent with CO concentration. Prior to the critical temperature, the reaction was smooth. The oxygen consumption rate grew between critical and crack temperature, which rose intensely after crack temperature. Meanwhile, the oxygen consumption rate of 1/3 of coking coal was lower than gas-fat coal.

3.4. Thermal Analysis of Oxidized Coal

Thermal analysis of gas-fat coal and 1/3 coking coal were carried out in DSC. Random sampling was adopted in all experiments to determine the sequence of all samples to avoid unexpected factors that may cause inaccuracy. Temperature versus heat flow with coal at a heating rate of 5 °C/min is illustrated in Figure 3.

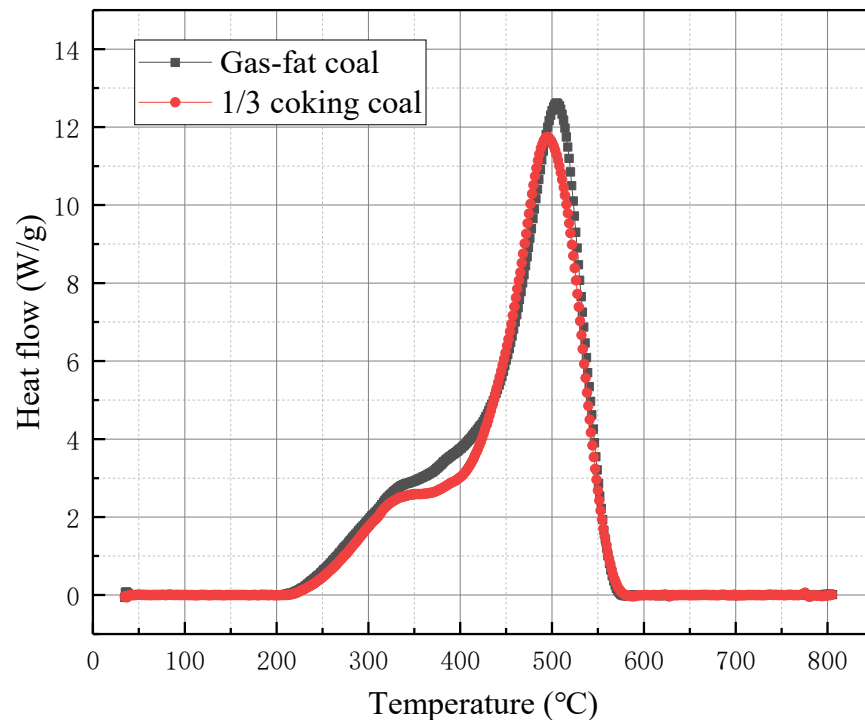


Figure 3. DSC curves of temperature versus heat flow at a heating rate of 5 °C/min.

Exothermic reaction occurred in the process of spontaneous coal combustion. The heat flow increased with the temperature rose. When the temperature reached a certain point where the fire occurred, the heat flow began to lessen. Gas-fat coal produced the amount of heat of 16.68 J/g from 230 to 560 °C, and 1/3 of coking coal generated 15.63 J/g from 270 to 560 °C. The heat flow of gas-fat coal was higher than that of 1/3 of coking coal.

3.5. Analysis of the Achar Differential and Coats-Redfern Integral Method

Various kinetic models have been applied to thermokinetic analysis to assess the thermal danger of the spontaneous combustion of oxidized coal in previous literature. The apparent activation energy (E_{α}), which reflects the energy required for a substance to react, is often adopted to evaluate the thermal safety of the substance. The higher its value is, the safer the substance will be. The value of E_{α} can be obtained by the Arrhenius equation shown in Equation (3) [46]:

$$\frac{d\alpha}{dt} = A \exp\left(-\frac{E_a}{RT}\right) f(\alpha) \quad (3)$$

Based on the Arrhenius equation, the Achar differential and Coats–Redfern integral model are described as follows [47]:

$$\ln\left(\frac{d\alpha}{f(\alpha)dT_{\alpha}}\right) = \ln\left(\frac{A}{\beta}\right) - \frac{E_{\alpha}}{RT_{\alpha}} \quad (4)$$

$$\ln\left[\frac{G(\alpha)}{T_{\alpha}^2}\right] = \ln\left(\frac{A}{E_{\alpha}\beta}\right) - \frac{E_{\alpha}}{RT_{\alpha}} \quad (5)$$

where α is the conversion rate, β is the heating rate, A is the pre-exponential factor, R is the gas constant which has a value of $8.314 \text{ J}/(\text{mol}\cdot\text{K})$, T_α is the temperature corresponding to α , and $f(\alpha)$ and $G(\alpha)$ are differential and integrated kinetic models, respectively. The five mechanism functions of $f(\alpha)$ and $G(\alpha)$ we chose are listed in Table 2 [48]. The different $f(\alpha)$ and $G(\alpha)$ equations are substituted into Equations (3) and (4), and the E_α values can be obtained by linear fitting of $1/T$ versus $\ln(d\alpha/f(\alpha)dT_\alpha)$ and $\ln(G(\alpha)/T_\alpha^2)$ [49]. The fitting curves of the two samples were shown in Figure 4. As can be seen from Figure 5 and Table 3, E_α values obtained by $f(\alpha)3$ and $G(\alpha)3$ are similar for both samples, which are regarded as optimal. The average values of E_α of gas-fat coal and 1/3 coking coal are 142.14 and $121.77 \text{ kJ}/\text{mol}$, respectively.

Table 2. Common mechanism functions.

| Number | Reaction Mechanism | Differential Function $f(\alpha)$ | Integral Function $G(\alpha)$ |
|--------|--|---|-------------------------------|
| 1 | First-order chemical reaction, $n = 1$ | $1 - \alpha$ | $-\ln(\alpha)$ |
| 2 | 1.5 order chemical reaction, $n = 1.5$ | $(1 - \alpha)^{3/2}$ | $2[(1 - \alpha)^{-1/2} - 1]$ |
| 3 | Third-order chemical reaction, $n = 1.5$ | $(1 - \alpha)^3$ | $[(1 - \alpha)^{-2} - 1]/2$ |
| 4 | 3D diffusion Z.-L.-T. equation | $3/2(1 - \alpha)^{4/3}[(1 - \alpha)^{-1/3} - 1]^{-1}$ | $[(1 - \alpha)^{-1/3} - 1]^2$ |
| 5 | Avrami-Eroféev, $n = 2$ | $1/2(1 - \alpha)[- \ln(1 - \alpha)]^{-1}$ | $[- \ln(1 - \alpha)]^2$ |

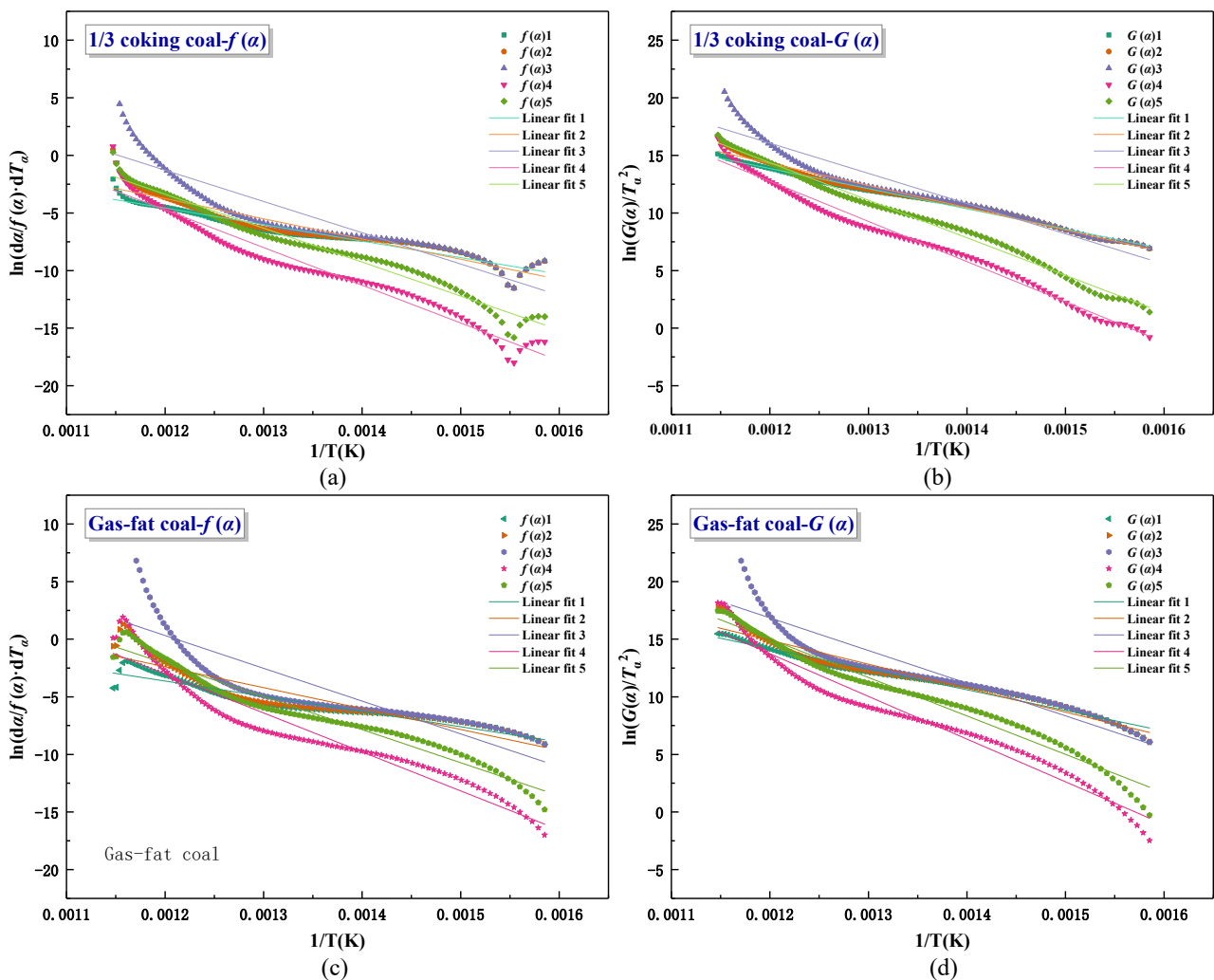


Figure 4. Fitting results for 1/3 coking coal and gas-fat coal. (a) 1/3 coking coal fitting by $f(\alpha)$; (b) 1/3 coking coal fitting by $G(\alpha)$; (c) Gas-fat coal fitting by $f(\alpha)$; (d) Gas-fat coal fitting by $G(\alpha)$.

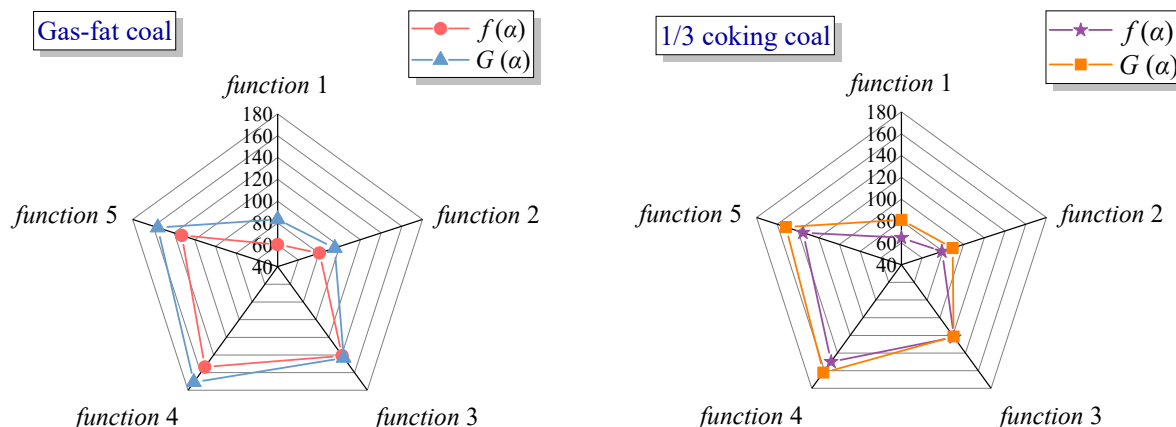


Figure 5. E_a values of 1/3 coking coal and gas-fat coal calculation by the Achar differential and Coats-Redfern Integral method with five functions.

Table 3. The E_a value obtained by multi-model fitting using the Achar differential and Coats-Redfern integral model.

| Sample | Number | E_a (kJ/mol) | | | |
|-----------------|--------|----------------|-------------|---------|------------|
| | | $f(\alpha)$ | $G(\alpha)$ | Average | Difference |
| Gas-fat coal | 1 | 60.19 | 83.25 | 71.72 | 23.06 |
| | 2 | 80.39 | 95.21 | 87.80 | 14.82 |
| | 3 | 141.00 | 143.28 | 142.14 | 2.29 |
| | 4 | 153.73 | 170.91 | 162.32 | 17.18 |
| | 5 | 132.67 | 155.73 | 144.20 | 23.06 |
| 1/3 coking coal | 1 | 64.71 | 81.17 | 72.94 | 16.47 |
| | 2 | 79.08 | 89.44 | 84.26 | 10.36 |
| | 3 | 122.20 | 121.34 | 121.77 | 0.86 |
| | 4 | 150.01 | 162.21 | 162.21 | 12.20 |
| | 5 | 135.12 | 151.59 | 151.59 | 16.47 |

3.6. Thermokinetic Multiple Linear Regression Analysis

The multiple linear regression method was employed for comparison and verification to confirm the accuracy of the results of the kinetic calculations [50]. The complex thermal decomposition of oxidized coal can be studied, and the reaction mechanism can be predicted using the multiple linear regression method. The autocatalytic reaction model shown in Equation (6) and the n -order reaction model shown in Equation (7) are commonly used in multiple linear regression [51].

$$\frac{d\alpha}{dt} = k_0 e^{-\frac{E_a}{RT}} (1 - \alpha)^{n1} (z + \alpha)^{n2} \quad (6)$$

$$\frac{d\gamma}{dt} = k \exp^{-\frac{E_a}{RT}} (\alpha - \gamma)^n \quad (7)$$

It is assumed that the thermal decomposition of oxidized coal is divided into two steps: A to B1 and B1 to B. Based on the DSC experimental data of 1/3 coking coal, the two stages were all simulated by the n -order model, and the results are shown in Figure 6. The consistency between the experimental and simulated curves indicates that the thermal decomposition reaction of 1/3 coking coal conforms to the two-step n -order reaction model. In addition, the heat production and heat production rates of B1 to B are more significant than those of A to B1, indicating that the second stage is dominant, and the reaction in the first stage promotes the reaction in the second stage.

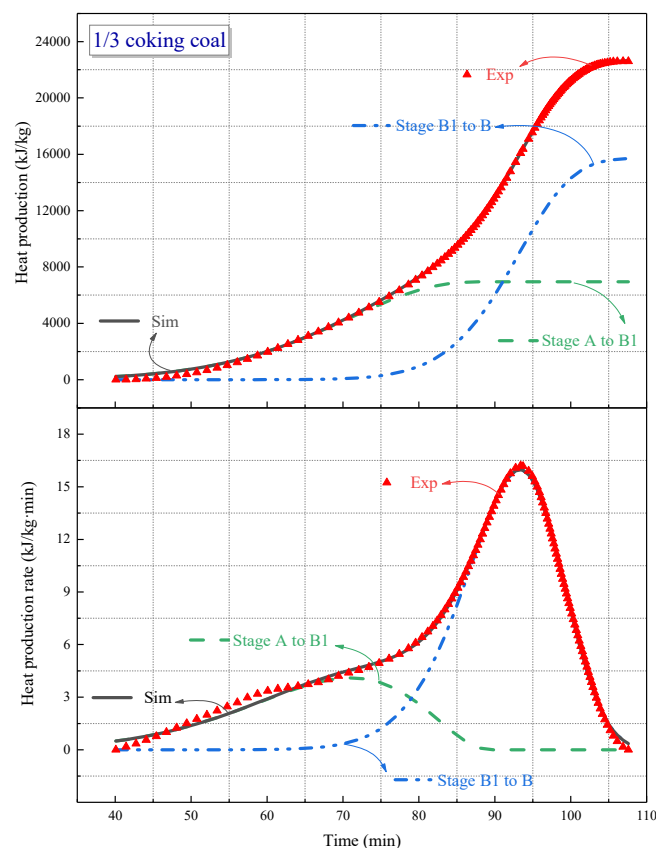


Figure 6. Heat production and heat production rate of 1/3 coking coal at heating rates of 5 °C/min obtained by experiments and simulations.

Multiple linear regression was also performed on gas-fat coal using the same model. The simulation results of the two samples are listed in Table 4. The results of gas-fat coal show that the E_a value for the first stage is 62.70 kJ/mol, and the E_a value is 140.36 kJ/mol in the second stage. The ΔH value of the first stage is 5890.231 J/g, while the value of the second stage is 17,890.451 J/g. For 1/3 coking coal, the E_a values of the two stages are 49.00 and 148.24 kJ/mol, and the ΔH values of the two stages are 6952.66 and 15,726.36 J/g. This also demonstrates that the reaction in the first stage with smaller apparent activation energy could proceed more easily; hence significant control measures for coal spontaneous combustion like foam, water mist, and composite gel could be conducted in this stage to break the continuous reaction [52]. Early detection of coal spontaneous combustion based on the above obtained characteristic parameters should also be emphasized appropriately to improve the control efficiency.

Table 4. Fitting parameters of multiple linear regressions for gas-fat coal and 1/3 coking coal.

| Parameters | Stage | $\ln(k_0)$ (1/s) | E_a (kJ/mol) | n | ΔH (J/g) |
|-----------------|-------|------------------|----------------|-------|------------------|
| Gas-fat coal | I | 4.946 | 62.70 | 1.342 | 5890.231 |
| | II | 15.685 | 140.36 | 0.954 | 17,890.451 |
| 1/3 coking coal | I | 2.170 | 49.00 | 0.709 | 6952.660 |
| | II | 16.928 | 148.24 | 1.046 | 15,726.360 |

4. Conclusions

Oxidized gas-fat coal and 1/3 coking coal had similar characteristics during spontaneous combustion. Index gases, oxygen consumption rates, and thermal release increased as the temperature rose. The CO concentration increased slowly before critical temperature and had a slow growth trend between critical and crack temperatures. Both the CO and

C₂H₄ concentrations increased straightly after the crack temperature. Heat flow continued to increase until the coal burnt to fire at temperatures of 490 and 510 °C of gas-fat coal and 1/3 coking coal, respectively. Both gas-fat coal and 1/3 coking coal fit the third-order chemical reaction mechanism function. The simulation results show that the thermal behavior of gas-fat coal and 1/3 coking coal could be accurately predicted by a two-stage reaction model. Two oxidized coals' E_a was calculated to be between 49.00 and 148.24 kJ/mol.

Author Contributions: Conceptualization, Y.T. and A.-C.H.; validation and methodology, W.-C.C. and A.-C.H.; formal analysis and resources, H.-L.Z. and J.-Y.Z.; writing—original draft preparation, Y.T., A.-C.H., and H.-L.Z.; writing—review and editing, A.-C.H. and C.-M.S.; project administration and funding acquisition, J.-Y.Z. and C.-M.S. All authors have read and agreed to the published version of the manuscript.

Funding: This work was supported by the National Key Research Development Program of China (No. 2021YFC3001203), the National Natural Science Foundation of China (No. 21927815), the Science and Technology Planning Project of Changzhou University (No. ZMF19020387), and the General Natural Science Research Project of Jiangsu Universities (No. 20KJD620001) for financial support.

Conflicts of Interest: The authors declare no conflict of interest.

References

1. Lu, X.; Deng, J.; Xiao, Y.; Zhai, X.; Wang, C.; Yi, X. Recent progress and perspective on thermal-kinetic, heat and mass transportation of coal spontaneous combustion hazard. *Fuel* **2022**, *308*, 121234. [[CrossRef](#)]
2. Liang, Y.; Zhang, J.; Wang, L.; Luo, H.; Ren, T. Forecasting spontaneous combustion of coal in underground coal mines by index gases: A review. *J. Loss Prev. Process Ind.* **2019**, *57*, 208–222. [[CrossRef](#)]
3. Zhang, J.; Xu, K.; Reniers, G.; You, G. Statistical analysis the characteristics of extraordinarily severe coal mine accidents (ESCMAs) in China from 1950 to 2018. *Process Saf. Environ. Prot.* **2020**, *133*, 332–340. [[CrossRef](#)]
4. Xu, Q.; Yang, S.; Yang, W.; Tang, Z.; Hu, X.; Song, W.; Zhou, B.; Yang, K. Secondary oxidation of crushed coal based on free radicals and active groups. *Fuel* **2021**, *290*, 120051. [[CrossRef](#)]
5. Taraba, B.; Michalec, Z. Effect of longwall face advance rate on spontaneous heating process in the gob area—CFD modelling. *Fuel* **2011**, *90*, 2790–2797. [[CrossRef](#)]
6. Melody, S.M.; Johnston, F.H. Coal mine fires and human health: What do we know? *Int. J. Coal Geol.* **2015**, *152*, 1–14. [[CrossRef](#)]
7. Biswal, S.S.; Gorai, A.K. Change detection analysis in coverage area of coal fire from 2009 to 2019 in Jharia Coalfield using remote sensing data. *Int. J. Remote Sens.* **2020**, *41*, 9545–9564. [[CrossRef](#)]
8. Chen, G.; Ma, X.; Lin, M.; Peng, X.; Yu, Z. Pollutant emission characteristics and interaction during low-temperature oxidation of blended coal. *J. Energy Inst.* **2016**, *89*, 40–47. [[CrossRef](#)]
9. Li, J.; Li, Z.; Yang, Y.; Duan, Y.; Xu, J.; Gao, R. Examination of CO, CO₂ and active sites formation during isothermal pyrolysis of coal at low temperatures. *Energy* **2019**, *185*, 28–38. [[CrossRef](#)]
10. Prodan, M.; Mitu, M.; Razus, D.; Oancea, D. Spark ignition and propagation properties of methane-air mixtures from early stages of pressure history. *Rev. Roum. Chim.* **2016**, *61*, 299–305.
11. Prodan, M.; Ghicioi, E.; Jurca, A.; Oancea, D. Ignition and propagation properties of coal dust-air-methane hybrid mixtures. *Rev. Roum. Chim.* **2021**, *66*, 25–32. [[CrossRef](#)]
12. Zhang, J.; Ren, T.; Liang, Y.; Wang, Z. A review on numerical solutions to self-heating of coal stockpile: Mechanism, theoretical basis, and variable study. *Fuel* **2016**, *182*, 80–109. [[CrossRef](#)]
13. Wang, H.; Dlugogorski, B.Z.; Kennedy, E.M. Coal oxidation at low temperatures: Oxygen consumption, oxidation products, reaction mechanism and kinetic modelling. *Prog. Energy Combust. Sci.* **2003**, *29*, 487–513. [[CrossRef](#)]
14. Chen, W.Y.; Shi, G.; Wan, S. Characterization of early-stage coal oxidation by temperature-programmed desorption. *Energy Fuels* **2008**, *22*, 3724–3735. [[CrossRef](#)]
15. Xin, H.H.; Wang, D.M.; Qi, X.Y.; Qi, G.S.; Dou, G.L. Structural characteristics of coal functional groups using quantum chemistry for quantification of infrared spectra. *Fuel Process. Technol.* **2014**, *118*, 287–295. [[CrossRef](#)]
16. Zheng, Y.; Li, Q.; Lin, B.; Zhou, Y.; Liu, Q.; Zhang, G.; Zhao, Y. Real-time analysis of the changing trends of functional groups and corresponding gas generated law during coal spontaneous combustion. *Fuel Process. Technol.* **2020**, *199*, 106237. [[CrossRef](#)]
17. Zhong, X.; Kan, L.; Xin, H.; Qin, B.; Dou, G. Thermal effects and active group differentiation of low-rank coal during low-temperature oxidation under vacuum drying after water immersion. *Fuel* **2019**, *236*, 1204–1212. [[CrossRef](#)]
18. Wang, D.M. *Mine Fire Science*; China University of Mining and Technology Press: Beijing, China, 2008. (In Chinese)
19. Qi, G.; Wang, D.; Zheng, K.; Xu, J.; Qi, X.; Zhong, X. Kinetics characteristics of coal low-temperature oxidation in oxygen-depleted air. *J. Loss Prev. Process Ind.* **2015**, *35*, 224–231. [[CrossRef](#)]
20. Li, Q.W.; Xiao, Y.; Wang, C.P.; Deng, J.; Shu, C.M. Thermokinetic characteristics of coal spontaneous combustion based on thermogravimetric analysis. *Fuel* **2019**, *250*, 235–244. [[CrossRef](#)]

21. Zhong, X.; Li, L.; Chen, Y.; Dou, G.; Xin, H. Changes in thermal kinetics characteristics during low-temperature oxidation of low-rank coals under lean-oxygen conditions. *Energy Fuels* **2017**, *31*, 239–248. [[CrossRef](#)]
22. Li, Y.; Zhao, H.; Song, Q.; Wang, X.; Shu, X. Influence of critical moisture content in lignite dried by two methods on its physicochemical properties during oxidation at low temperature. *Fuel* **2018**, *211*, 27–37. [[CrossRef](#)]
23. Liang, Y.; Tian, F.; Guo, B.; Liu, Z. Experimental investigation on microstructure evolution and spontaneous combustion properties of aerobic heated coal. *Fuel* **2021**, *306*, 121766. [[CrossRef](#)]
24. Zhang, Y.N.; Chen, L.; Deng, J.; Zhao, J.Y.; Li, H.T.; Yang, H. Influence of granularity on thermal behaviour in the process of lignite spontaneous combustion. *J. Therm. Anal. Calorim.* **2019**, *135*, 2247–2255. [[CrossRef](#)]
25. Deng, J.; Xiao, Y.; Li, Q.; Lu, J.; Wen, H. Experimental studies of spontaneous combustion and anaerobic cooling of coal. *Fuel* **2015**, *157*, 261–269. [[CrossRef](#)]
26. Song, Z.; Wu, D.; Jiang, J.; Pan, X. Thermo-solutal buoyancy driven air flow through thermally decomposed thin porous media in a U-shaped channel: Towards understanding persistent underground coal fires. *Appl. Therm. Eng.* **2019**, *159*, 113948. [[CrossRef](#)]
27. Su, H.; Zhou, F.; Song, X.; Qiang, Z. Risk analysis of spontaneous coal combustion in steeply inclined longwall gobs using a scaled-down experimental set-up. *Process Saf. Environ. Prot.* **2017**, *111*, 1–12. [[CrossRef](#)]
28. Xia, T.; Zhou, F.; Liu, J.; Kang, J.; Gao, F. A fully coupled hydro-thermo-mechanical model for the spontaneous combustion of underground coal seams. *Fuel* **2014**, *125*, 106–115. [[CrossRef](#)]
29. Song, Z.Y.; Zhu, H.Q.; Tan, B.; Wang, H.Y.; Qin, X.F. Numerical study on effects of air leakages from abandoned galleries on hill-side coal fires. *Fire Saf. J.* **2014**, *69*, 99–110. [[CrossRef](#)]
30. Tang, Y.; Zhong, X.; Li, G.; Yang, Z.; Shi, G. Simulation of dynamic temperature evolution in an underground coal fire area based on an optimized Thermal–Hydraulic–Chemical model. *Combust. Theor. Model.* **2019**, *23*, 127–146. [[CrossRef](#)]
31. Zhang, Y.; Zhang, Y.; Li, Y.; Li, Q.; Zhang, J.; Yang, C. Study on the characteristics of coal spontaneous combustion during the development and decaying processes. *Process Saf. Environ. Prot.* **2020**, *138*, 9–17. [[CrossRef](#)]
32. Qi, G.; Lu, W.; Qi, X.; Zhong, X.; Cheng, W.; Liu, F. Differences in smoldering characteristics of coal piles with different smoldering propagation directions. *Fire Saf. J.* **2018**, *102*, 77–82.
33. Xiao, Y.; Ye, X.X.; Liu, K.H.; Chen, L.G. Transformation law of key functional groups in the process of coal secondary oxidation. *J. China Coal Soc.* **2021**, *46*, 989–1000.
34. Zhao, J.; Deng, J.; Wang, T.; Song, J.; Zhang, Y.; Shu, C.M.; Zeng, Q. Assessing the effectiveness of a high-temperature-programmed experimental system for simulating the spontaneous combustion properties of bituminous coal through thermokinetic analysis of four oxidation stages. *Energy* **2019**, *169*, 587–596. [[CrossRef](#)]
35. Yi, L.; Feng, J.; Qin, Y.H.; Li, W.Y. Prediction of elemental composition of coal using proximate analysis. *Fuel* **2017**, *193*, 315–321. [[CrossRef](#)]
36. Wang, Y.S.; Xue, G.F.; Bao, J.F.; Ren, Y.M. Analysis on residual coke during medium maintenance of No.6 blast furnace of Wusteel. *Iron Steel* **2016**, *50*, 20–24.
37. Slepetiene, A.; Slepetyus, J.; Liaudanskiene, I. Chemical composition of differently used Terric Histosol. *Zemdirbyste* **2010**, *97*, 25–32.
38. Wu, H.; Yang, N.; Tang, Y.; Jiang, J.C.; Huang, A.C. Thermal Stability Evaluation of T152 Emulsifier on the Modification Influence of Fireworks Propellant. *Processes* **2022**, *10*, 1606. [[CrossRef](#)]
39. Zhang, C.Z.; Xie, L.J.; Tang, Y.; Li, Y.; Jiang, J.C.; Huang, A.C. Thermal Safety Evaluation of Silane Polymer Compounds as Electrolyte Additives for Silicon-Based Anode Lithium-Ion Batteries. *Processes* **2022**, *10*, 1581. [[CrossRef](#)]
40. Qi, D.; Wu, S.; Li, S.; Zhao, G.; Xing, J.; Kang, S.; Wang, Q.; Gao, W. Enrichment Characteristics, Occurrence and Origin of Valuable Trace Elements in Lignite from Linchang Coal Mine, Guangxi, China. *J. Geosci. Environ. Prot.* **2021**, *9*, 133–150. [[CrossRef](#)]
41. Ma, Y. Multiscale Fractal Characterization of Pore Structure for Coal in Different Rank Using Scanning Electron Microscopy and Mercury Intrusion Porosimetry. *Processes* **2022**, *10*, 1577. [[CrossRef](#)]
42. Chen, X.; Li, H.; Wang, Q.; Zhang, Y. Experimental investigation on the macroscopic characteristic parameters of coal spontaneous combustion under adiabatic oxidation conditions with a mini combustion furnace. *Combust. Sci. Technol.* **2018**, *190*, 1075–1095. [[CrossRef](#)]
43. Dong, X.W.; Wen, Z.C.; Wang, F.S.; Meng, Y.N. Law of gas production during coal heating oxidation. *Int. J. Min. Sci. Technol.* **2019**, *29*, 617–620. [[CrossRef](#)]
44. Lin, B.; Li, Q.; Zhou, Y. Research advances about multi-field evolution of coupled thermodynamic disasters in coal mine goaf. *J. China Coal Soc.* **2021**, *46*, 1715–1725.
45. Deng, J.; Wu, X.; Cheng, C. Experimental study on explosion of multicomponent combustibility gases containing CH₄, CO and C₂H₄. *Coal Mine Mod.* **2007**, *5*, 63–65.
46. Xie, L.J.; Jiang, J.C.; Huang, A.C.; Tang, Y.; Liu, Y.C.; Zhou, H.L.; Xing, Z.X. Calorimetric evaluation of thermal stability of organic liquid hydrogen storage materials and metal oxide additives. *Energies* **2022**, *15*, 2236. [[CrossRef](#)]
47. Yang, Y.P.; Jiang, J.C.; Huang, A.C.; Tang, Y.; Liu, Y.C.; Xie, L.J.; Zhang, C.Z.; Wu, Z.H.; Xing, Z.X.; Yu, F. 3-(Trifluoromethyl) benzoylacetonitrile: A multi-functional safe electrolyte additive for LiNi_{0.8}Co_{0.1}Mn_{0.1}O₂ cathode of high voltage lithium-ion battery. *Process Saf. Environ. Prot.* **2022**, *160*, 80–90. [[CrossRef](#)]
48. Yang, Y.; Ding, L.; Xu, L.; Tsai, Y.T. Effect of metal chloride on thermal decomposition of nitrocellulose. *Case Stud. Therm. Eng.* **2021**, *28*, 101667. [[CrossRef](#)]

49. Zhang, C.Z.; Jiang, J.C.; Huang, A.C.; Tang, Y.; Xie, L.J.; Zhai, J.; Xing, Z.X. A novel multifunctional additive strategy improves the cycling stability and thermal stability of SiO/C anode Li-ion batteries. *Process Saf. Environ. Prot.* **2022**, *164*, 555–565. [[CrossRef](#)]
50. Yao, C.; Liu, Y.C.; Wu, J.; Tang, Y.; Zhai, J.; Shu, C.M.; Jiang, J.C.; Xing, Z.X.; Huang, C.F.; Huang, A.C. Thermal Stability Determination of Propylene Glycol Sodium Alginate and Ammonium Sulfate with Calorimetry Technology. *Processes* **2022**, *10*, 1177. [[CrossRef](#)]
51. Huang, A.C.; Huang, C.F.; Xing, Z.X.; Jiang, J.C.; Shu, C.M. Thermal hazard assessment of the thermal stability of acne cosmeceutical therapy using advanced calorimetry technology. *Process Saf. Environ. Prot.* **2019**, *131*, 197–204. [[CrossRef](#)]
52. Shao, Z.; Wang, D.; Wang, Y.; Zhong, X.; Tang, X.; Hu, X. Controlling coal fires using the three-phase foam and water mist techniques in the Anjialing Open Pit Mine, China. *Nat. Hazards* **2015**, *75*, 1833–1852. [[CrossRef](#)]